RSC Advances

ROYAL SOCIETY OF CHEMISTRY

www.rsc.org/advances

Influence of biomaterial nanotopography on the adhesive and elastic properties of *Staphylococcus aureus* cells

S Aguayo [1], A Strange [1], N Gadegaard [2], MJ Dalby [3], L Bozec [1]*

[1] Department of Biomaterials and Tissue Engineering, UCL Eastman Dental Institute, University College London, London, UK
[2] Division of Biomedical Engineering, School of Engineering, University of Glasgow, UK
[3] Centre for Cell Engineering; Institute of Molecular, Cell and Systems Biology, University of Glasgow, UK

Corresponding author:

*** Sebastian Aguayo**

Division of Biomaterials and Tissue Engineering

UCL Eastman Dental Institute

University College London

256 Gray's Inn Road, London

WC1X 8LD - UK

E: Sebastian.aguayo.13@ucl.ac.uk

Abstract:

Despite the well-known beneficial effects of biomaterial nanopatterning on host tissue integration, the influence of controlled nanoscale topography on bacterial colonisation and infection remains unknown. Therefore, the aim of the present study was to determine the nanoscale effect of surface nanopatterning on biomaterial colonisation by *S. aureus,* utilising AFM nanomechanics and single-cell force spectroscopy (SCFS). Nanoindentation of *S. aureus* bound to planar (PL) and nanopatterned (SQ) polycarbonate (PC) surfaces suggested two distinct areas of mechanical properties, consistent with a central bacterial cell surrounded by a capsullar component. Nevertheless, no differences in elastic moduli were found between bacteria bound to PL and SQ, suggesting a minor role of nanopatterning in bacterial cell elasticity. Furthermore, SCFS demonstrated increased adhesion forces and work between *S. aureus* and SQ surfaces at 0s and 1s contact times. Although WLC modelling showed similarities in contour lengths for attachment to both surfaces, Poisson analysis suggests increased short-range forces for the *S. aureus*-SQ interactions. In the case of *S. aureus*-PL, long-range forces were found to not only be dominant but also repulsive in nature, which may help explain the reduced adhesion forces observed during AFM probing. In conclusion, although surface nanopatterning does not significantly influence the elasticity of attached bacterial cells, it was found to promote the early-adhesion of *S. aureus* cells to the biomaterial surface.

1. Introduction:

Biomaterials are currently being employed in modern medicine for the augmentation or replacement of missing or diseased tissues[1, 2]. More specifically, they are used in a wide range of medical applications such as catheters, artificial heart valve replacements, and orthopaedic and dental implants[3]. In recent years, many surface modifications have been incorporated into the design of biomaterials in the hope of improving their biological activity and host tissue integration[3, 4]. Amongst these improvements, controlled nanopatterning of the biomaterial surface has been shown to directly influence human stem cell proliferation and differentiation, giving it an important advantage compared to uncontrolled topographies and planar surfaces[5, 6]. Despite these positive effects, the effect of biomaterial nanopatterning on bacterial surface colonisation remains unknown[7].

After implantation, many bacterial strains have demonstrated an increased capacity of adhering to the surface of biomaterials and artificial implants[8]. As implant surface infection has been repeatedly shown to be detrimental for biomaterial-host tissue integration and can lead to complications as severe as replacement surgery, there is current focus on understanding the process of bacterial adhesion to biomaterial surfaces[9]. Amongst others, *Staphylococcus aureus* has shown an increased likelihood to colonise and infect implants in humans and its presence is related to negative clinical prognosis[10-12]. *S. aureus* is a facultative anaerobic and coagulase-positive Gram positive cocci[13], with the ability to cause disease in humans and animals ranging from bone infection to pneumonia and septicaemia[14]. Some of the many virulence factors of *S. aureus* are the presence of

capsule and surface proteins, which promote adhesion to biotic and abiotic surfaces and aid in the process of biofilm formation[15]. In recent years, *S. aureus* has demonstrated increased antibiotic resistance and as a result, novel antibacterial and anti-adhesive approaches are currently being explored in hopes of developing new strategies against biomaterial surface infection[16-18].

Atomic force microscopy (AFM) has proven to be a valuable tool for the *in-vitro* characterisation of cellular and sub-cellular mechanics[19]. Particularly for microbiology, it allows the possibility to study the nanomechanics of living bacterial cells in buffer conditions without the need for prior sample preparation[20]. Using this methodology, it is possible to assess the elastic properties of surface-bound bacteria by indenting the bacterial surface with an AFM cantilever[21]. Furthermore, by employing approaches such as single-cell force spectroscopy (SCFS), bacterial adhesion to biological and non-biological surfaces can be studied in the nano- and pico-meter ranges[22-24].

Several studies have used AFM to probe the nanomechanics of *S. aureus* and its adhesion to substrates and other cells[25-27]. However, little is known regarding the influence that nanopatterning exerts on *S. aureus* adhesion and early-colonisation of the implant surface. As a result, the aim of this study was to determine the nanoscale effect of surface nanopatterning on *S. aureus* biomaterial colonisation by utilising AFM nanoindentation and single-cell force spectroscopy (SCFS) techniques.

2. Experimental:

2.1. Polycarbonate surface characterisation

Two distinct engineered polycarbonate (PC) surfaces were employed throughout the study. Nanopatterned PC surfaces, consisting of 120nm pits with 300nm centre-centre separation in a square arrangement (SQ), were obtained with a previously reported protocol[5]. A planar PC surface (PL) was employed as a smooth control.

Previous to any measurements, nanopatterned surfaces were prepared and cleaned by sonication in dH_2O for 5mins, washed with 70% ethanol and dried under N_2 airflow. Characterisation of surface topography was obtained by AFM imaging (Dimension 3100, Bruker, Santa Barbara, USA) employing intermittent contact mode in air, utilising MSNL-10 (Bruker, USA) cantilevers with a scanning rate of 1.0Hz. Average surface roughness (R_a) was determined using height images obtained during AFM scanning (n = 3), and processed using proprietary NanoScope Analysis 1.5 software (Bruker, USA). For bacterial experiments, surfaces were placed in a UV-chamber and sterilised with a 20min cycle (BR-506, UVC Light Products, UK). Surface hydrophilicity was determined after surface sterilisation, by contact angle measurements with deionised water (dH_2O) utilising a Cam 200 Optical Contact Angle Meter (Biolin Scientific, Germany). A single 5µl droplet was applied to the surfaces, and the average angle of contact over 10 seconds was measured and recorded (n = 3).

2.2. Bacterial cultures

Stocks of *S. aureus* (strain 8325-4) were maintained at -80°C in 85% glycerol/15% tryto-soy broth (TSB, Oxoid Ltd, UK) medium. For experiments, *S. aureus* were grown in TSB for 16hrs at 37°C and aeration until stationary phase. Subsequently, 100µl of bacterial suspension was diluted 10-fold in phosphate-buffer saline (PBS 1x, Lonza, Belgium) and harvested at 5000rpm for 1min (Eppendorf 5417R, UK). Resulting pellets were re-suspended in 1mL PBS and utilised immediately for experiments.

2.3. Sample preparation for scanning electron microscopy/focused ion beam (SEM-FIB) milling and imaging.

To obtain images of *S. aureus* colonisation of PC surfaces, a 500µl droplet of bacterial suspension was incubated on each surface for 10min, rinsed with PBS to remove unattached cells, and fixed immediately with 4% glutaraldehyde. Samples were then dehydrated with 10min serial washes in 50, 70, 90 and 100% ethanol, and sputter coated with gold. Imaging was carried out with an XB1540 (Carl Zeiss, Germany) SEM-FIB system with an acceleration voltage of 10kV at magnifications of 50,000x and 100,000x. FIB milling was carried out with a 30kV:20mA gallium beam probe, by tilting the sample 54° and performing serial linear millings on *S. aureus* cells until exposing the bacterial-surface interface.

2.4. Sample preparation for AFM

2.4.1. AFM imaging and bacterial nanomechanics

To attach single *S. aureus* cells onto substrates for imaging and nanomechanics, a 20µl droplet of bacterial suspension was deposited onto each PC surface and incubated for 10min. For imaging, samples were washed after incubation with dH_2O and softly dried under N_2 airflow. For nanoindentation, samples were washed with PBS to remove unattached cells, and re-suspended with 100µl of TRIS buffer (Sigma-Aldrich, UK). For all nanomechanic experiments, bacterial cells were maintained submerged in TRIS buffer throughout experimentation.

Both imaging and force-volume mapping of the bacterial surface of *S. aureus* were obtained by employing a JPK Nanowizard system (JPK Instruments, Germany) mounted on an inverted optical microscope (Olympus IX71, Olympus, Japan). Imaging was carried out with a NCS35 cantilever (MikroMasch, USA) in intermittent contact mode in air, tuned at ~110KHz. Set point and gain values were adjusted in-situ during scanning for image optimisation. Images were obtained at 512x512pixels with an average scanning rate of 0.5Hz.

For force-volume mapping, MSNL-10 cantilevers with a spring constant of ~0.1N/m were used. After locating an isolated attached bacterium, force-curves were obtained (constant speed of 2µm/s and a loading force of 3nN) at random points of the cell centre and perimeter of each bacterium. Six independent *S. aureus* cells were indented and analysed per surface. As minimal adhesion between the cantilever and bacterial cell was recorded and an indentation depth of ~50nm was

obtained, Young's modulus (YM) was determined from the extension curve by applying the Hertzian model as previously described in the literature[28]:

$$F = \frac{4ER^{1/2}\delta^{3/2}}{3(1-v^2)} \quad \text{(Equation 1)}$$

where F is force, E is the Young's modulus, R is the radius of the indenter, δ is indentation distance and v is the Poisson's ratio of the indented sample (considered as 0.5).

2.4.2. Single-cell force spectroscopy (SCFS)

For SCFS experiments, customised colloidal probes were fabricated in order to immobilise *S. aureus* cells by utilising a protocol previously published[26]. Briefly, the end of a tipless cantilever (NP-O10, Bruker, Santa Barbara, USA) was brought into contact with a thin layer of UV-curable glue (Loctite, UK) for 10s. Subsequently, the glue-coated tip was approached to a ~10μm silica microsphere (Whitehouse Scientific, UK) with a maximum loading force of 0.5nN for 3min. Upon retraction, effective attachment of the silica bead was observed by optical microscopy. Functionalised cantilevers were then UV-cured for 10mins, and correct placing of the microsphere was assessed by SEM imaging (Philips XL30 FEG SEM, FEI, Eindhoven, Netherlands). As a next step, functionalised cantilevers were coated for 1hr with a solution of 4mg/ml dopamine hydrochloride (poly-DOPA) in 10mM TRIS buffer (pH8.0), washed with dH_2O and dried with N_2. All cantilevers were calibrated using thermal tuning (~0.3N/m spring constants), and stored at 4°C until AFM experiments.

To functionalise colloidal probes with living *S. aureus* cells, cantilevers were mounted onto the AFM and submerged into a 20µl droplet of bacterial suspension. The probe was then brought into contact with an isolated cell, with a loading force of 0.5nN for ~3mins until attachment was observed. Cantilevers were then retracted, transferred above the PC surface and submerged in TRIS buffer being careful not to dehydrate the *S. aureus* probe. Experiments were carried out with a loading force of 0.5nN, a constant speed of 2µm/s, and surface delay times of 0s and 1s. Each of the *S. aureus* functionalised probes were utilised only for a single experiment and discarded thereafter. Four independent *S. aureus* probes were utilised for each surface (totalling 8 probes).

2.5. Data analysis:

All obtained images and force curves were analysed using the JPK Data Processing Software v.5.1.8 (JPK Instruments, Germany). For nanomechanics, histograms and median (Mdn) values were obtained for each surface and contact time, and significance was determined by applying the non-parametric Mann-Whitney test ($p<0.05$). From SCFS force curves, maximum adhesion force (nN) between the bacterial cell and cantilever was obtained as the lowest negative value for force during the retraction phase, and overall adhesion work (aJ) was obtained by integrating the area under the retraction curve. Unbinding peaks observed during retraction were fitted with the worm-like chain (WLC) model as previously described assuming a persistent length of 0.36nm[29]. Finally, a Poisson analysis of *S.*

aureus-PC unbinding was performed employing a previously published approach, to decouple adhesion into short-range (F_{SR}) and long-range (F_{LR}) forces[30].

3. Results and discussion:

3.1. Characterisation of bacterial adhesion onto PC surfaces

AFM imaging of PC substrates demonstrated different topographies for the PL and SQ surfaces **(Figure 1)**. SQ exhibited a very distinct patterning, with clearly defined nanopits at regular intervals consistently throughout the surface, which contrasted strongly with the smooth topography observed for PL. AFM surface cross sections of SQ further showed rounded nanopits with an average diameter of 99± 6nm (n=20) and a depth of ~70nm. Also, R_a measurements showed an increased surface roughness of 13.7±0.8nm for SQ surfaces compared to 0.4±0.0nm for PL ones. No difference was found in surface wettability, with values for PL and SQ at 80.6±2.7° and 80.3±1.5° respectively. However these values do indicate that PC surfaces, irrespective of patterning, are slightly hydrophilic which has been previously shown to favour staphylococcal attachment[31].

Images of surface-bound *S. aureus* cells were successfully obtained with intermittent contact mode AFM imaging. More specifically, it was possible to observe the *S. aureus* cell surrounded by a microcapsule **(Figure 2.a and b)**. This area appears to not only surround the bacterial cell but to also cover its surface partially, consistent with previous AFM observations which employed a similar *S. aureus* strain[32]. Further phase contrast imaging, which has been previously used to differentiate cell from capsule in streptococcal species[33], was used to demonstrate differences in physico-mechanical properties between the bacterial cell and adjacent area **(Figure 2.c)**. Height images obtained with force-volume mapping in buffer are also consistent with this bacterial morphology, and although resolution is

not as high as with intermittent contact imaging, the bacteria-capsule structure can still be clearly observed in the corresponding pixel map **(Figure 4.a)**. Interestingly, previous research suggests that although *S. aureus* strain 8325-4 carries a serotype-5 capsule gene, it is defective in capsule expression[34, 35]. However, Coldren and colleagues found very similar morphological characteristics in a serotype-8 capsule-positive *S. aureus* strain when imaged with AFM under comparable conditions[36]. Serotype-5 and serotype-8 bacterial capsules are considered to have similar characteristics[34], and therefore it is possible that the strain is effectively expressing a capsule-like structure.

Although careful preparation was used, it was not possible to image the *S. aureus* capsule under the SEM-FIB, suggesting that it is destroyed or lost during sample dehydration and preparation **(Figure 3)**. Subsequently, upon exposing the *S. aureus*-PC interface with FIB milling, only minor contact between bacteria and surface could be observed and therefore it is believed that the bacteria-substrate interaction is mostly mediated by capsule rather than by the bacterial cell itself. Overall, imaging suggests that *S. aureus* capsule does not only account for a significant part of bacterial size observed in AFM imaging, but most importantly, it also increases the effective contact area between the bacterium and PC surface during surface attachment.

3.2. Underlying substrate topography does not influence the nanomechanical properties of surface-bound *S. aureus*

The elastic properties of surface-bound *S. aureus* were obtained in force-volume mode by performing a number of force curves on the bacterial surface. Two distinct

mechanical behaviours were observed for *S. aureus*, consistent with the presence of a stiffer cell body surrounded by capsule of decreased stiffness **(Figure 4.b)**. This observation was consistent throughout measurements for *S. aureus* cells attached to both studied PC surfaces. YM for the bacterial cell was found to be 2.20MPa for PL and 4.14MPa for SQ, in the range of previously reported values for *S. aureus* 8325-4 elasticity[37]. However, surrounding the central bacterium, an area with significantly reduced YM of 116.58kPa for PL and 92.89kPa for SQ was observed ($p<0.05$) **(Figure 4.c and d)**.

Regarding the influence of the underlying surface on of *S. aureus* nanomechanics, no significant differences were found in YM between bacteria bound to PL and SQ substrates ($p>0.05$)**(Figure 4.c and d)**. As AFM imaging demonstrated that a typical *S. aureus* cell directly interacts with a number of nanopits on the SQ surface, any effect that nanotopography may have on bacterial cell elasticity should be clearly noticeable at the single-cell level. However, both *S. aureus* cell and capsule nanomechanics were not affected by the presence or absence of surface nanopatterning. It is also possible that nanopatterning may only exert a localised effect on elasticity in the vicinity of the bacteria-nanopattern interface, and therefore it cannot be explored by solely indenting the top region of attached *S. aureus* cells.

3.3. Adhesion forces between *S. aureus*-PC surfaces are increased by the presence of surface nanopatterning

To analyse the effect of surface nanopatterning on the early colonisation of *S. aureus*, functionalised AFM bacterial probes were constructed and probed against

PC surfaces at 0s and 1s contact times **(Figures 5 and 6)**. Adhesion force and work between *S. aureus* and PL surfaces were found to be <0.05nN and <0.05aJ at 0s surface contact times delays. However, increasing the contact time to 1s raised these values to 0.11nN and 5.01aJ respectively ($p<0.0001$). Adhesion forces between *S. aureus* and SQ surfaces was increased at both time points compared to PL, with values of 0.10nN at 0s and 0.23nN at 1s surface delay times ($p<0.0001$). A similar increase was observed for the work of adhesion, with values of 4.28aJ and 18.75aJ for 0s and 1s respectively ($p<0.0001$). Altogether, these results suggest that both contact time and surface nanopatterning directly influence the early-adhesion of *S. aureus* to PC surfaces. In the literature, SCFS of *S. aureus* strain 8325-4 has been previously employed to measure its adhesion with *Candida albicans* hyphae and yeast cells and fibronectin-functionalised AFM cantilevers[38, 39]. In both cases, reported adhesion forces were of higher magnitudes than the ones observed in the present study between *S. aureus* and PC. As these studies examined specific receptor-ligand interactions between *S. aureus* and biological substrates, it is possible to hypothesise that the reduced adhesion forces observed for the unbinding of *S. aureus*-PC, irrespective of patterning, is a reflection of a lack of specificity between the bacterial cell and surface. It also remains possible that increased loading forces were employed in these studies, which has been shown to promote bacterial adhesion to substrates[40].

Representative force curves obtained for both PL and SQ surfaces can be observed in **Figure 7.a**. In both cases, 'sawtooth-like' unbinding peaks indicative of specific adhesion between the probe and surface were clearly observed throughout

measurements. These unbinding events were fitted with the WLC model, yielding contour length values predominantly situated in the 50-400nm range **(Figure 7.b)**. The number of unbinding peaks found for SQ (n=942) was slightly increased compared to PL (n=889). Interestingly, it was possible to fit multiple curves to the contour length distributions of both PL and SQ. PL surfaces displayed peaks at 140nm, 270nm and 358nm; while SQ surfaces were also found to have similar peaks at lengths of 147nm, 253nm, and 380nm respectively **(Figure 7.b)**. This data suggests that a range of surface and/or capsule receptors are involved in the adhesion between *S. aureus* and PC surfaces, with no important differences found regarding the presence or absence of nanopatterning. In a recent study, average contour lengths between *S. aureus* and titanium (Ti) implant surfaces were reported at 314.1±9.3nm[26]. Ti is more hydrophilic than PC and biomaterial surface hydrophilicity has been previously shown to favour bacterial adhesion[31]. However, it has yet to be determined if contour lengths observed for S*. aureus*-PC unbinding correspond to the same Ti-binding receptors stretched to different lengths, or if they reflect another surface adhesion mechanism.

Furthermore, Poisson analysis of *S. aureus*-PC unbinding was carried out to decouple overall adhesion forces into F_{SR} and F_{LR}. PL surfaces were found to have a F_{SR} of -0.08±0.02nN, while SQ surfaces showed an increased value of -1.42±0.02nN (**Table 1**). Interestingly, F_{LR} for PL surfaces was found to be a positive value of 0.38±0.25nN, and as such it indicates that the overall long-range forces acting between *S. aureus* and PL are repulsive in nature. Increased F_{SR} between *S. aureus*-

SQ surfaces paired with a repulsive F_{LR} in *S. aureus*-PL may help explain the reduced adhesion force and work observed in the latter case.

Overall, the use of SCFS was an effective approach to study the early-colonisation of *S. aureus* onto PC surfaces at the nanoscale. In biomaterial infection, early bacterial colonisers are believed to come into contact with the surface with minimal to no external loading forces being applied. Therefore, in this PC-based model of biomaterial nanopatterning, loading forces for *S. aureus* probes were reduced (0.5nN) to avoid deformation of the bacterial cell during probing. By utilising this 'zero-force contact' approach, it is believed that the influence of AFM probing on adhesion values can be kept to a minimum. High loading forces would therefore not effectively recreate the physiological process of bacterial adhesion, as they would be promoting the interaction between bacteria and surface. This effect was recently demonstrated by Chen et al, where the adhesion between *S. aureus* strain 8325-4 and a glass surface was found to be proportional to the loading force applied[40].

In the literature, the capsule has been considered to play an active role in bacterial attachment to biomaterial surfaces[41, 42]. Considering the early contact times utilised in this study (0 and 1s), it is believed that adhesion between *S. aureus* and PL and SQ surfaces at these time points is mostly mediated by the interaction between the capsule and substrate. Although nanopatterning theoretically reduces the contact area between cell and surface, adhesion was found to be increased for SQ surfaces compared to PL. It is hypothesised that this observation is a result of the physical interaction between the capsule and the roughness conferred by the nanopatterned surface. This mechanical retention might increase bacterial

attachment to the surface during probe retraction, yielding increased adhesive forces probed with the AFM. Also, the interaction between capsule and/or surface receptors and the surface were observed, in the form of specific unbinding peaks. At this stage however, we do not believe that it is possible to pinpoint the exact receptors involved in the adhesion of *S. aureus* to PC surfaces; nevertheless, due to the predicted contour lengths observed with WLC modelling (~150-400nm), we believe that a range of receptors are involved in this interaction[26].

In the past, surfaces with nanoscale topographies were found to possess improved antibacterial properties against *S. aureus*, when bacteria are cultured for <1hr and macro-scale bacterial attachment assays such as fluorescence microscopy and spread plate methods were employed[7, 43-45]. However, results from the present study suggest that nanopatterning increases the colonisation of biomaterial surfaces at early contact times (0 and 1s). Although bacterial adhesion to surfaces is a crucial initial phase[46], it does not account on its own for the entire process of biomaterial colonisation[45]. Therefore, it remains possible that although attachment of *S. aureus* to nanopatterned surfaces is initially increased at very short time points, bacteria may not be able to effectively colonise the surface due to reduced proliferation capabilities or decreased capsule secretion at increased contact times. Although contact times of ≤1s may be short in relation to the lifetime of a biomaterial infection process, early-colonising bacteria could potentially become a 'base-layer' for the attachment of secondary bacteria at increased time points[47]. Future efforts should focus on further understanding the in-vivo relevance of early biomaterial colonisation by *S. aureus*, and if promoting or inhibiting this initial bacterium-

surface interaction can aid in the search for novel ways to control biofilm formation without compromising the increased biological properties of nanopatterned surfaces.

Conclusion:

Both nanoindentation and AFM SCFS were found to be powerful tools to study the nanomechanics of living *S. aureus* cells in buffer conditions. Imaging of surface bound *S. aureus* showed the presence of adjacent capsule regardless of surface patterning, which was found to have reduced elasticity compared to the central bacterial cell. No surface-induced changes in bacterial nanomechanics were found in *S. aureus* attached to PL and SQ. However, SCFS with *S. aureus* functionalised probes demonstrated increased adhesion forces and work between bacteria and SQ surfaces. Poisson analysis suggests that this is due to higher short-range forces between *S. aureus*-SQ and repulsive long-range forces between *S. aureus*-PL. Overall, surface nanotopography was found to influence *S. aureus* attachment to PC surfaces at early time points, and further research should evaluate is this effect is observable at increased contact times and in other biomaterial surfaces of clinical relevance.

Acknowledgements:

This work has been funded by the Becas-Chile PhD Scholarship Programme.

Figure legends:

Figure 1: Characterisation of planar (PL) and nanopatterned (SQ) polycarbonate (PC) surfaces. 2x2μm AFM 3D reconstruction images of (A) PL and (B) SQ demonstrate marked topographical differences between both surfaces. (C) and (D) correspond to AFM height scans for PL and SQ respectively, from which surface cross sections were obtained (E) (2x2μm scans). From these cross sections, it is possible to observe nanopit depth and patterning on the SQ surface. (F) Although surface roughness was increased in SQ compared to PL surfaces, no differences were found in regards to surface wettability as both substrates were found to display a slightly hydrophilic behaviour.

Figure 2: AFM intermittent contact imaging of *S. aureus* 8325-4 adhered to PL and SQ surfaces. 3D reconstruction images of S. *aureus* attached to (A) PL and (B) SQ surfaces. It is possible to observe the S. *aureus* cell surrounded and partially covered by capsule (inset arrows) (C) Phase contrast image obtained for the bacterium imaged in (A), which evidences distinct structural composition and physic-mechanical properties for both the *S. aureus* cell (cross) and capsule (stars). The capsule is seen to not only surround the cell but also cover it partially.

Figure 3: SEM-FIB imaging and milling of the *S. aureus*-PC interface. Imaging of *S. aureus* cells attached to PL (A, B) and SQ (C, D) surfaces before and after FIB milling, respectively (A and C 50,000x; B and D 100,000x). *S. aureus* capsule is absent due to it being destroyed during sample preparation, nevertheless, a minor degree of interaction can still be observed between bacterial cells and PC surfaces after FIB milling.

Figure 4: Nanomechanics of surface-bound *S. aureus* cells attached to PL and SQ in buffer. (A) 3D reconstruction image obtained during a *S. aureus* force-volume map, in which both the bacterial cell and capsule (arrow) can be observed. (B) 16x16pixel stiffness map on the surface of a *S. aureus* cell attached to a PL surface. An area of decreased stiffness can be observed surrounding the bacterial cell (asterisk). Values for Young's modulus (YM) obtained with the Hertzian model for (C) the bacterial cell and (D) capsule are shown (n=6 independent cells per group). A marked difference is observed between the two regions, with the bacterial cell showing values in the MPa range and

capsule being in the kPa range. No significant differences in YM were found between PL and SQ, suggesting that surface nanotopography does not influence the mechanics of *S. aureus* cells ($p>0.05$, Mann-Whitney).

Figure 5: Adhesion forces and work between living *S. aureus* and PC surfaces at short contact times. Histogram of adhesion forces and work recorded between *S. aureus*-functionalised AFM probes and PL and SQ surfaces, with a surface delay of 0s. For SQ, both parameters were significantly increased compared to PL surfaces ($p<0.05$). The number of non-adhesive events per group is indicated in the upper left corner of each histogram.

Figure 6: Adhesion forces and work between living *S. aureus* and PC surfaces at increased contact times. Histogram of adhesion forces and work recorded between *S. aureus*-functionalised AFM probes and PL and SQ surfaces, with a surface delay of 1s. Increasing the contact time to 1s increased adhesion forces and work in both studied surfaces ($p<0.05$). Similar to 0s contact times, both parameters were also found to be increased in SQ compared to PL surfaces ($p<0.05$).

Figure 7: Worm-like chain (WLC) modelling of force-extension peaks observed during *S. aureus*-PC unbinding. (A) Representative retraction curves observed during between *S. aureus* probes and PL and SQ surfaces. Single unbinding events can be observed in both cases, as indicated by the arrows. Insets represent AFM deflection images of each surface (2x2μm scans). (B) WLC modelling yielded multiple peaks for contour lengths in both PL and SQ, as observed in the corresponding histograms.

References:

1. N. Huebsch and D. J. Mooney, *Nature*, 2009, **462**, 426-432.
2. B. D. Ratner and S. J. Bryant, *Annual review of biomedical engineering*, 2004, **6**, 41-75.
3. N. Logan and P. Brett, *Stem cells international*, 2013, **2013**, 361637.
4. F. J. O'Brien, *Materials Today*, 2011, **14**, 88-95.
5. M. J. Dalby, N. Gadegaard, R. Tare, A. Andar, M. O. Riehle, P. Herzyk, C. D. Wilkinson and R. O. Oreffo, *Nature materials*, 2007, **6**, 997-1003.
6. M. Estevez, E. Martinez, S. J. Yarwood, M. J. Dalby and J. Samitier, *Journal of biomedical materials research. Part A*, 2015, **103**, 1659-1668.
7. Z. Jahed, P. Lin, B. B. Seo, M. S. Verma, F. X. Gu, T. Y. Tsui and M. R. Mofrad, *Biomaterials*, 2014, **35**, 4249-4254.
8. K. Subramani, R. E. Jung, A. Molenberg and C. H. Hammerle, *The International journal of oral & maxillofacial implants*, 2009, **24**, 616-626.
9. S. Svensson, M. Forsberg, M. Hulander, F. Vazirisani, A. Palmquist, J. Lausmaa, P. Thomsen and M. Trobos, *International journal of nanomedicine*, 2014, **9**, 775-794.
10. C. R. Arciola, D. Campoccia, P. Speziale, L. Montanaro and J. W. Costerton, *Biomaterials*, 2012, **33**, 5967-5982.
11. A. Lee and H. L. Wang, *Implant dentistry*, 2010, **19**, 387-393.
12. L. G. Harris, S. J. Foster and R. G. Richards, *European cells & materials*, 2002, **4**, 39-60.
13. F. D. Lowy, *The New England journal of medicine*, 1998, **339**, 520-532.
14. M. A. Holmes and R. N. Zadoks, *Journal of mammary gland biology and neoplasia*, 2011, **16**, 373-382.
15. K. O'Riordan and J. C. Lee, *Clinical microbiology reviews*, 2004, **17**, 218-234.
16. P. Loskill, P. M. Pereira, P. Jung, M. Bischoff, M. Herrmann, M. G. Pinho and K. Jacobs, *Biophysical journal*, 2014, **107**, 1082-1089.
17. R. A. McKendry, *Biochemical Society transactions*, 2012, **40**, 603-608.
18. G. Francius, O. Domenech, M. P. Mingeot-Leclercq and Y. F. Dufrene, *Journal of bacteriology*, 2008, **190**, 7904-7909.
19. Y. F. Dufrene, *Trends in microbiology*, 2015, **23**, 376-382.
20. S. Aguayo, N. Donos, D. Spratt and L. Bozec, *Nanotechnology*, 2015, **26**, 062001.
21. H. K. Webb, V. K. Truong, J. Hasan, R. J. Crawford and E. P. Ivanova, *Journal of microbiological methods*, 2011, **86**, 131-139.
22. A. V. Taubenberger, D. W. Hutmacher and D. J. Muller, *Tissue Eng Part B Rev*, 2013.
23. A. Beaussart, S. El-Kirat-Chatel, P. Herman, D. Alsteens, J. Mahillon, P. Hols and Y. F. Dufrene, *Biophysical journal*, 2013, **104**, 1886-1892.
24. R. M. Sullan, J. K. Li, P. J. Crowley, L. J. Brady and Y. F. Dufrene, *ACS nano*, 2015, **9**, 1448-1460.
25. E. S. Ovchinnikova, B. P. Krom, H. J. Busscher and H. C. van der Mei, *BMC Microbiology*, 2012, **12**, 281.
26. S. Aguayo, N. Donos, D. Spratt and L. Bozec, *Journal of dental research*, 2015.

27. B. M. Peters, E. S. Ovchinnikova, B. P. Krom, L. M. Schlecht, H. Zhou, L. L. Hoyer, H. J. Busscher, H. C. van der Mei, M. A. Jabra-Rizk and M. E. Shirtliff, *Microbiology*, 2012, **158**, 2975-2986.
28. C. Formosa, M. Grare, E. Jauvert, A. Coutable, J. B. Regnouf-de-Vains, M. Mourer, R. E. Duval and E. Dague, *Scientific reports*, 2012, **2**, 575.
29. P. Herman, S. El-Kirat-Chatel, A. Beaussart, J. A. Geoghegan, T. J. Foster and Y. F. Dufrene, *Molecular microbiology*, 2014, **93**, 356-368.
30. Y. Chen, H. J. Busscher, H. C. van der Mei and W. Norde, *Applied and environmental microbiology*, 2011, **77**, 5065-5070.
31. N. P. Boks, H. J. Busscher, H. C. van der Mei and W. Norde, *Langmuir*, 2008, **24**, 12990-12994.
32. T. Tollersrud, T. Berge, S. R. Andersen and A. Lund, *APMIS : acta pathologica, microbiologica, et immunologica Scandinavica*, 2001, **109**, 541-545.
33. H. V. Rukke, I. K. Hegna and F. C. Petersen, *Molecular oral microbiology*, 2012, **27**, 95-108.
34. E. R. Wann, B. Dassy, J. M. Fournier and T. J. Foster, *FEMS microbiology letters*, 1999, **170**, 97-103.
35. B. Kneidinger, K. O'Riordan, J. Li, J. R. Brisson, J. C. Lee and J. S. Lam, *The Journal of biological chemistry*, 2003, **278**, 3615-3627.
36. F. M. Coldren, E. L. Palavecino, N. H. Levi-Polyachenko, W. D. Wagner, T. L. Smith, B. P. Smith, L. X. Webb and D. L. Carroll, *Journal of biomedical materials research. Part A*, 2009, **89**, 402-410.
37. Y. Chen, W. Norde, H. C. van der Mei and H. J. Busscher, *mBio*, 2012, **3**.
38. E. S. Ovchinnikova, B. P. Krom, H. J. Busscher and H. C. van der Mei, *BMC Microbiol.*, 2012, **12**, 281.
39. C. P. Xu, N. P. Boks, J. de Vries, H. J. Kaper, W. Norde, H. J. Busscher and H. C. van der Mei, *Applied and environmental microbiology*, 2008, **74**, 7522-7528.
40. Y. Chen, A. K. Harapanahalli, H. J. Busscher, W. Norde and H. C. van der Mei, *Applied & Environmental Microbiology*, 2014, **80**, 637-643.
41. Y. H. An and R. J. Friedman, *Journal of biomedical materials research*, 1998, **43**, 338-348.
42. R. Baselga, I. Albizu and B. Amorena, *Veterinary microbiology*, 1994, **39**, 195-204.
43. K. Huo, X. Zhang, H. Wang, L. Zhao, X. Liu and P. K. Chu, *Biomaterials*, 2013, **34**, 3467-3478.
44. S. D. Puckett, E. Taylor, T. Raimondo and T. J. Webster, *Biomaterials*, 2010, **31**, 706-713.
45. K. Anselme, P. Davidson, A. M. Popa, M. Giazzon, M. Liley and L. Ploux, *Acta biomaterialia*, 2010, **6**, 3824-3846.
46. K. A. Whitehead, J. Colligon and J. Verran, *Colloids and surfaces. B, Biointerfaces*, 2005, **41**, 129-138.
47. M. Otto, *Annual review of medicine*, 2013, **64**, 175-188.

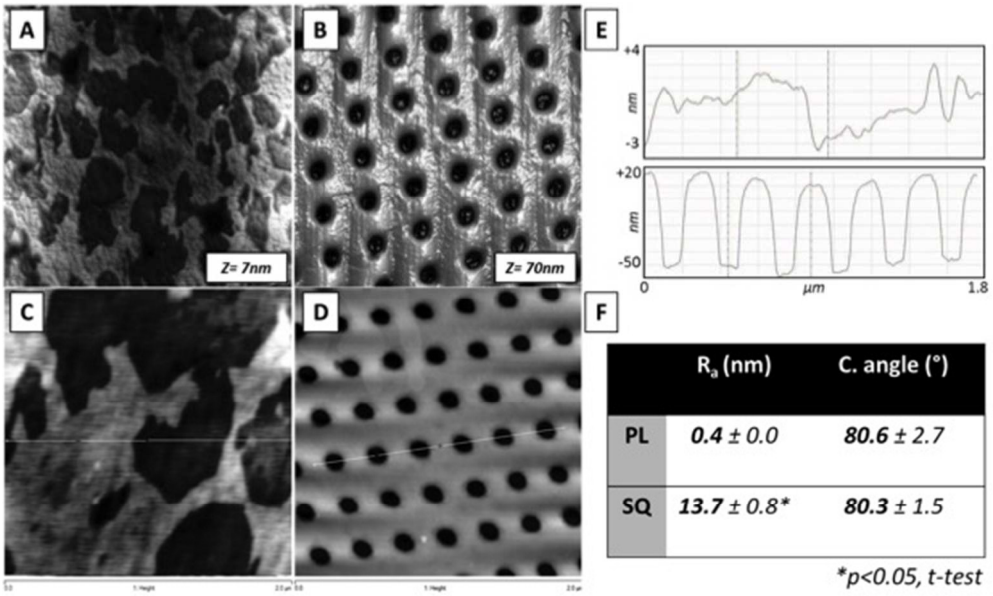

	R_a (nm)	C. angle (°)
PL	***0.4*** ± 0.0	***80.6*** ± 2.7
SQ	***13.7*** ± 0.8*	***80.3*** ± 1.5

*p<0.05, t-test

219x134mm (72 x 72 DPI)

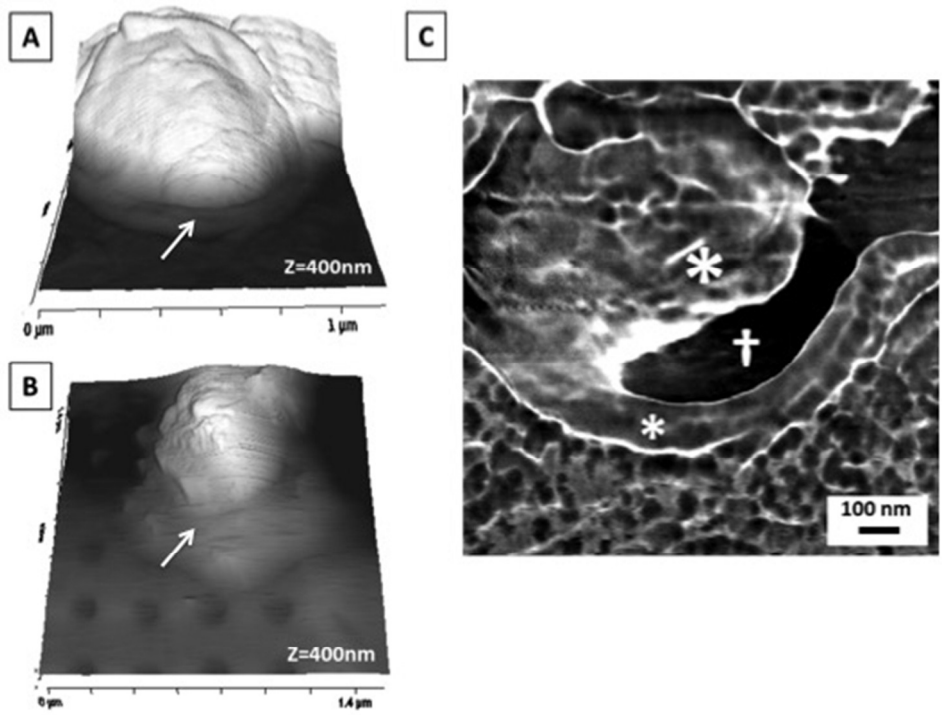

194x147mm (72 x 72 DPI)

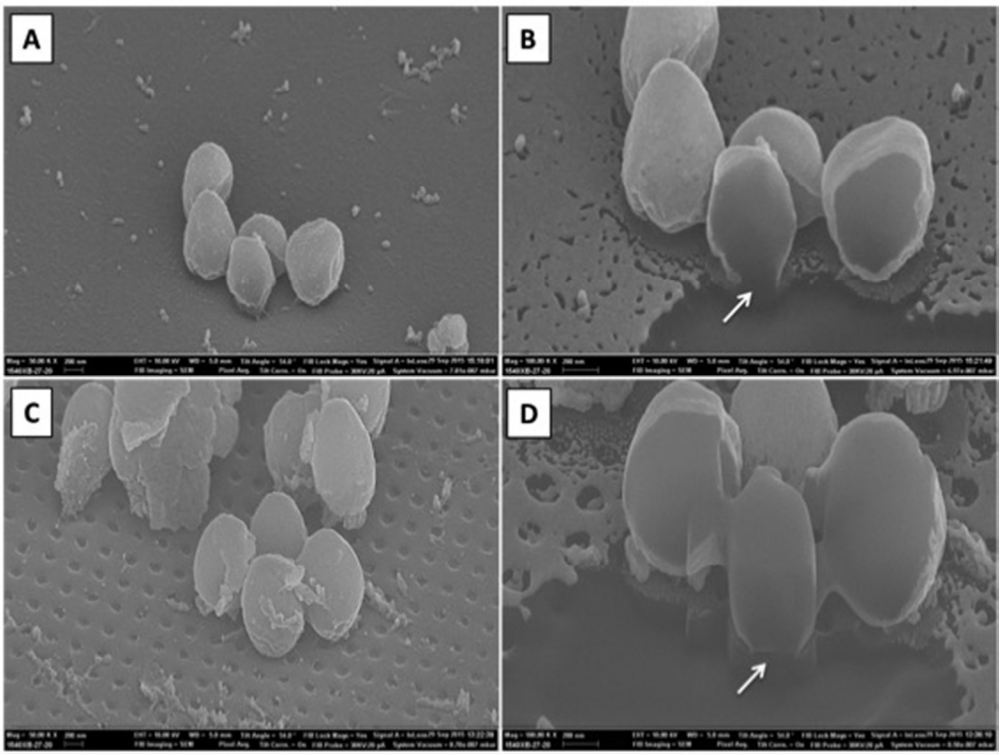

200x151mm (72 x 72 DPI)

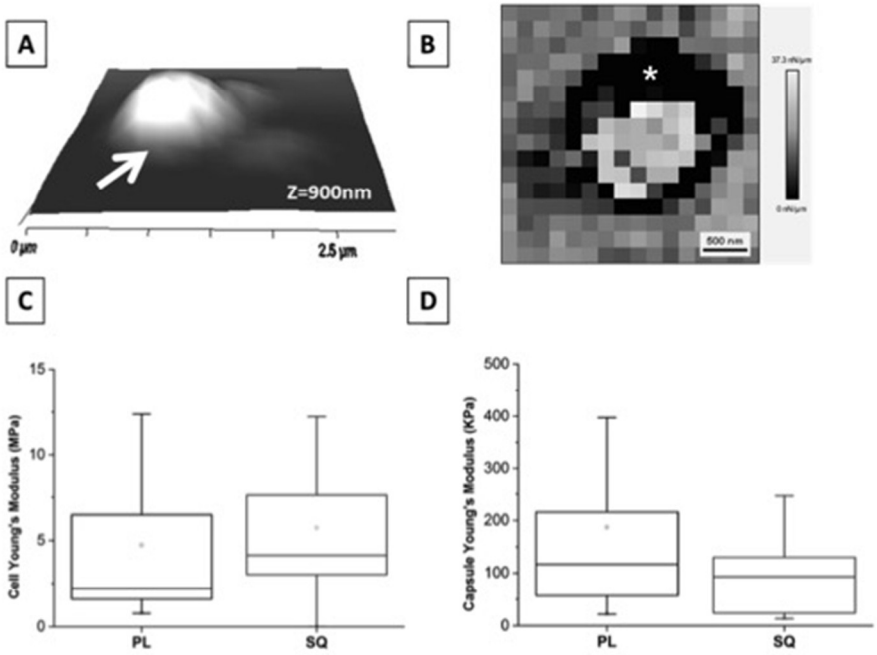

202x141mm (72 x 72 DPI)

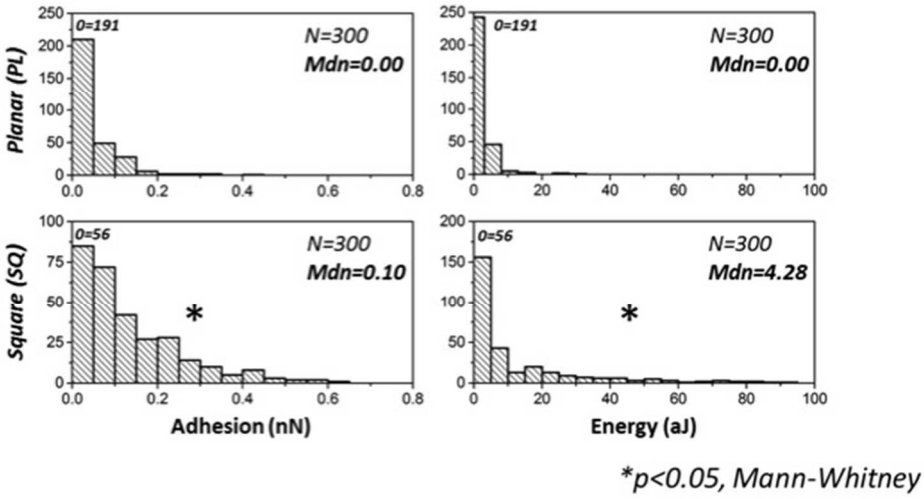

237x125mm (72 x 72 DPI)

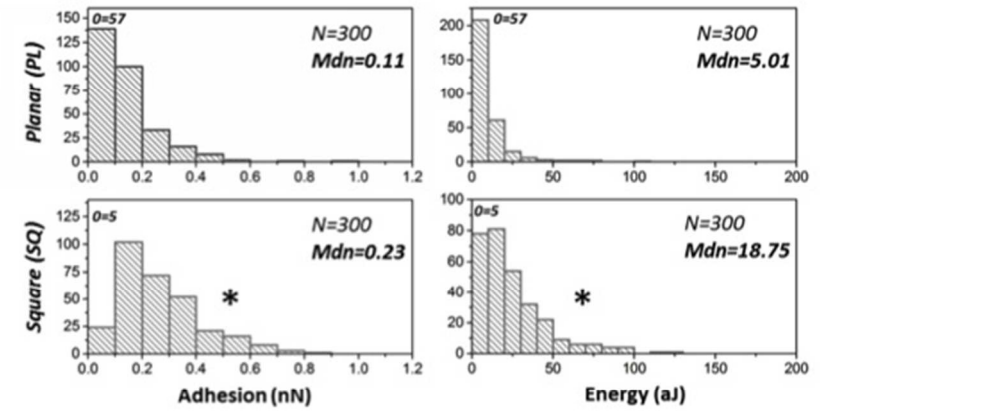

*p<0.05, Mann-Whitney

234x117mm (72 x 72 DPI)

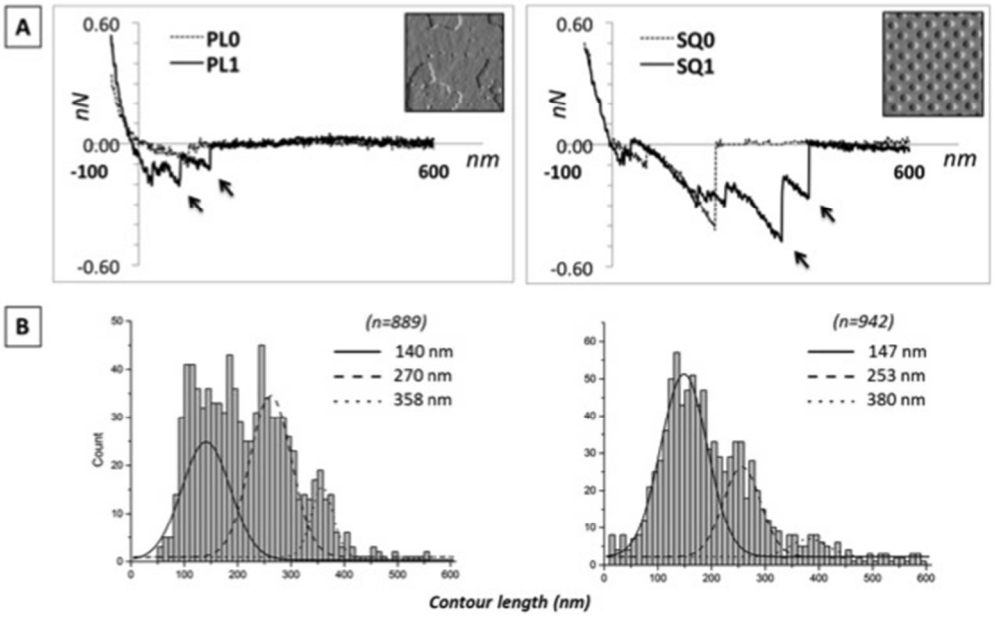

224x141mm (72 x 72 DPI)

TABLE 1: Poisson analysis of *S. aureus* unbinding from PL and SQ surfaces in buffer

Surface	Specific (F_{SR})		Non-specific (F_{LR})	
	Mean (nN)	*SE*	*Mean (nN)*	*SE*
PL	**-0.08**	*0.02*	**0.38**	*0.25*
SQ	**-1.42**	*0.02*	**-0.23**	*0.01*